Acta Crystallographica Section D
Biological Crystallography
ISSN 0907-4449

High-resolution X-ray structure of the rabbit histidine triad nucleotide-binding protein 1 (rHINT1)–adenosine complex at 1.10 Å resolution

Rafał Dolot,* Magdalena Ozga, Agnieszka Krakowiak and Barbara Nawrot

Department of Bioorganic Chemistry, Centre of Molecular and Macromolecular Studies of the Polish Academy of Sciences, 90-363 Łódź, Poland

Correspondence e-mail: rdolot@cbmm.lodz.pl

Received 4 October 2010
Accepted 25 April 2011

PDB Reference: rHINT1–adenosine complex, 3qgz.

Histidine triad nucleotide-binding protein 1 (HINT1) represents the most ancient and widespread branch in the histidine-triad protein superfamily. HINT1 plays an important role in various biological processes and has been found in many species. Here, the first complete structure of the rabbit HINT1–adenosine complex is reported at 1.10 Å resolution, which is one of the highest resolutions obtained for a HINT1 structure. The final structure has an $R_{\rm cryst}$ of 14.25% ($R_{\rm free}$ = 16.77%) and the model exhibits good stereochemical qualities. A detailed analysis of the atomic resolution data allowed an update of the details of the protein structure in comparison to previously published data.

1. Introduction

Histidine-triad nucleotide-binding protein 1 (HINT1) belongs to a histidine-triad (HIT) protein superfamily that has a characteristic C-terminal active-site motif H*X*H*X*H*XX*, where *X* is a hydrophobic residue (Brenner, 2002). HIT enzymes are an ubiquitous superfamily that consists of primarily mononucleotide and dinucleotide hydrolases and nucleotide transferases (Brenner, 2002). The HIT superfamily has been divided into five distinct branches by a phylogenic study of HIT proteins (Kijas *et al.*, 2006; Ahel *et al.*, 2006). HINT proteins have been described as the most conserved members of the HIT superfamily, with nucleotide hydrolase activity. HINT homologues are present in a wide variety of organisms including the metazoan, plant, fungal and bacterial kingdoms (Bieganowski *et al.*, 2002; Korsisaari *et al.*, 2003; Parks *et al.*, 2004; Chou *et al.*, 2005; Bardaweel *et al.*, 2010; Wu *et al.*, 2010; Guranowski *et al.*, 2011). The second branch of the HIT superfamily are the FHIT (fragile histidine triad) proteins, which are found only in eukaryotes, with representative sequences in human and yeast, and have been reported to be tumour suppressors (Ohta *et al.*, 1996). Human FHIT protein is an Ap_3A hydrolase (Barnes *et al.*, 1996). Moreover, this enzyme exhibits phosphoramidase activity towards adenosine-5′-phosphoimidazolide (AMP-Im) and adenosine-5′-phospho-*N*-methylimidazolide (AMP-*N*-MeIm; Huang *et al.*, 2005). The third branch contains aprataxin, which is mutated in the disease ataxia-oculomotor apraxia type 1 (Moreira *et al.*, 2001; Date *et al.*, 2006) and possesses phosphoramidase and Ap_4A hydrolase activity and DNA/RNA-binding affinity (Kijas *et al.*, 2006). The fourth branch contains the GalT (galactose-1-phosphate uridynyltransferase) proteins, which have low overall sequence similarity to HINT1 but have quite similar three-dimensional structure (Brenner *et al.*, 1997). The last branch contains the scavenger mRNA-decapping enzyme Dcsp/DCS-1, which exhibits 7-methyl-GpppG hydrolase

activity (Liu *et al.*, 2002). The strongly conserved sequences of HINT proteins suggest their fundamental role in cell metabolism. HINT1 is expressed in multiple tissues and is present both in the nucleus and cytoplasm, but its exact cellular function has still not been precisely defined.

In vitro studies indicate that human HINT1 is able to bind various nucleotides, *e.g.* AMP, ADP and the diadenosine polyphosphates Ap_3A and Ap_4A (Lima *et al.*, 1996). Rabbit HINT1 (rHINT1) also binds selected purine nucleosides and nucleotides (Brenner *et al.*, 1997). HINT proteins demonstrate phosphoramidase activity for adenosine-5′-*O*-monophosphoramidate (AMP-NH_2; Bieganowski *et al.*, 2002), firstly acting as efficient aminoacyl-adenylate hydrolases and then as acyl-adenylate hydrolases. Lysyl-adenylate generated by lysyl-tRNA synthetase (LysRS) has also been suggested to be a substrate of HINT1 (Chou & Wagner, 2007; Chou *et al.*, 2007). Ability to hydrolyze the P—N bond in nucleoside phosphoramidates has been demonstrated in studies of the conversion of PSI-7851 (a potent 2′-deoxy-2′-fluoro-2′-*C*-methyluridine-5′-monophosphate prodrug) with potential anti-HCV activity both *in vitro* and *in vivo* (Murakami *et al.*, 2010). Recently conducted research confirmed that rabbit HINT1 is able to catalyze the desulfuration of 5′-*O*-phosphorothioylated nucleosides (Krakowiak *et al.*, 2007; Ozga *et al.*, 2010).

HINT1 is involved in transcription regulation, cell-cycle control and induction of apoptosis. HINT1 regulates the activity of microphthalmia transcription factor (MITF), which plays an important role in the growth of mastocytes and melanocytes (Lee *et al.*, 2004). Inhibition of AP-1 (activator protein 1) is exerted by binding of HINT1 to the POSH–JNK2 complex and inhibition of c-Jun phosphorylation (Wang *et al.*, 2007). HINT1 is also involved in regulation of the ubiquitously expressed transcription factor USF2 (Lee & Razin, 2005) and NFκB, which is involved in tumour development (Wang *et al.*, 2009). HINT1 interacts with other proteins, *e.g.* human μ-opioid receptor, which is a G-protein-coupled receptor that mediates analgesia, euphoria and other important central and peripheral neurological functions (Guang *et al.*, 2004). HINT1 binds to the pontin–reptin–β-catenin–TCF4 complex and thus inhibits TCF4 transcription factor activity, which is part of the Wnt–β-catenin–TCF4 signalling pathway that plays a role in cell survival, proliferation and differentiation (Weiske & Huber, 2005). HINT1 is also associated with the Tip60–pontin–reptin complex, which is involved in the transcription process (Weiske & Huber, 2006) and is a negative regulator of transcription of Src, which decreases the stability of the $p27^{KIP1}$ cyclin-dependent kinase inhibitor by forming a complex with transcription factor Sp1 on the promoter site of Src (Cen *et al.*, 2009).

Recent studies suggest that mammalian HINT1 modulates apoptosis in cancer cells and is a potential tumour suppressor (Su *et al.*, 2003; Li *et al.*, 2006; Wang *et al.*, 2007, 2009; Zhang *et al.*, 2009). Down-regulation of the expression of HINT1 significantly increased cell resistance to apoptosis induced by UV treatment, indicating its potential role in cellular hormesis and possible function in tumour suppression (Weiske & Huber, 2006; Wang *et al.*, 2009; Hsieh *et al.*, 2009). High mRNA levels of HINT1, together with IFITM2, LGALS3BP, STOLM2 and c-Myc, have been observed to be associated with reduced risk of disease development, including metastasis in Ewing's sarcoma (Zambelli *et al.*, 2010).

The first HINT1 crystal structure was published in 1996 (Lima *et al.*, 1996); it was initially described as an inhibitor of protein kinase C (Pearson *et al.*, 1990) and further as PKCI (protein kinase C-interacting; Klein *et al.*, 1998). Finally, the 'HINT' name was used after structural analysis (Brenner *et al.*, 1997). At present, 13 HINT1 structures are available in the PDB, six from human (Lima *et al.*, 1996, 1997), five from rabbit (Brenner *et al.*, 1997; Krakowiak *et al.*, 2004) and two from *E. coli* (Bardaweel *et al.*, 2010), both in the apo state (Lima *et al.*, 1996) and in complex with selected ligands: substrate analogues or the products of their hydrolysis (Lima *et al.*, 1997; Krakowiak *et al.*, 2004; Bardaweel *et al.*, 2010). To date, the highest reported data resolution for wild-type HINT1 protein is 1.80 Å (PDB entry 1rzy; Krakowiak *et al.*, 2004) and 1.50 Å (PDB entry 1kpf; Lima *et al.*, 1997) for the rabbit and human clones, respectively. Recently, three structures of rHINT1 cysteine mutants (C38A, C84A and C38/84A) have been published at atomic resolution (PDB codes 3o1c, 3o1x and 3o1z; Ozga *et al.*, 2010).

The structure of rHINT1 is characterized as a general α+β fold and further subclassified as an α+β meander fold. The monomer consists of a five-stranded antiparallel β-sheet and two α-helices: a short helix α1 localized close to the N-terminus and a long helix α2 localized between the β3 and β5 strands. Helices α1 (residues 18–24) and α2 (residues 68–86) pack on opposite sides of the β-sheet, which is wrapped around the longest helix (Fig. 1). X-ray crystal structure and

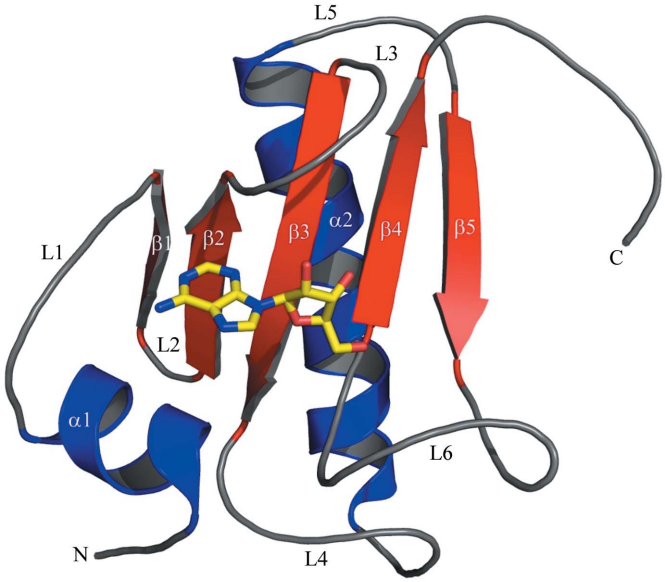

Figure 1
Cartoon diagram of rHINT1 (PDB entry 3qgz). Structural elements are indicated in blue (α-helices) and red (β-strands). The active-site location is indicated by the bound adenosine (shown in stick representation). Secondary-structure elements were assigned with *DSSP* (Kabsch & Sander, 1983). This figure was created with *PyMOL* v.0.99 (DeLano Scientific, Palo Alto, California, USA).

size-exclusion chromatography analyses have revealed that the human HINT1 protein exists as a homodimer (Chou *et al.*, 2005; Lima *et al.*, 1996, 1997). Two monomers make up a dimer, which forms a ten-stranded antiparallel β-sheet, while the α2 helix from one monomer is localized opposite the $\alpha2'$ helix from the other monomer (Fig. 2). Each of the constituent monomers contains a well separated active site that does not participate in the dimer interface (Boulanger & Kantrowitz, 2003).

The nucleotide-binding pocket is formed by loops L1, L3 and L5, helix α1 and a fragment of the β-sheet. The purine base-binding site is localized between the helix and the L1 loop and mostly consists of conserved hydrophobic residues. Loop L3 is responsible for binding the ribose residue. Loop L5 is in contact with the sugar and phosphate moieties. Conserved polar residues, including His112 and His114, from the HIT motif are involved in binding the α-phosphate moiety (Lima *et al.*, 1996, 1997). The cleft is not localized on the dimer-contact interface and each of the monomeric components can independently bind one molecule of the nucleoside. Nevertheless, the C-terminus of each monomer makes a range of contacts with the adjacent monomer in close proximity to the active site, including hydrogen-bond interactions between Gly126 and Arg119′ and Asn122′ from the second chain. In addition, the C-terminal fragment of one monomer is involved in closing the binding pocket from the second monomer using the Trp123 residue, which is situated at the opposite position to helix α1, but these residues do not interact with the nucleoside molecule.

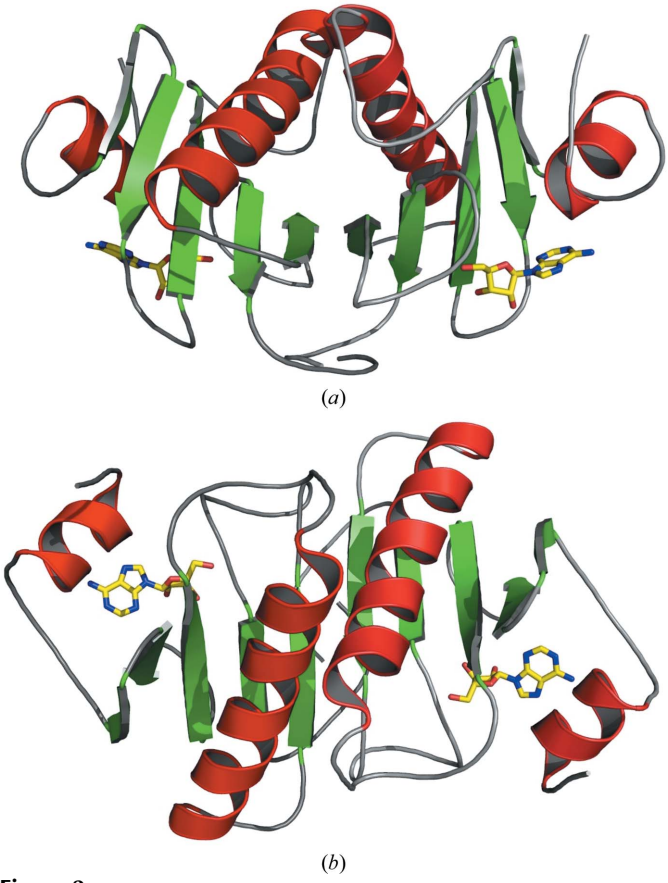

Figure 2
(*a*) Cartoon representation of the rHINT1 dimer (based on PDB entry 3qgz). Each of the monomers is shown in a darker and lighter colour scheme. (*b*) The same dimer structure after a 90° rotation. This figure was created with *PyMOL* v.0.99 (DeLano Scientific, Palo Alto, California, USA).

Table 1
Statistics of X-ray data collection.

Values in parentheses are for the highest resolution shell.

Beamline	MAX-lab I911-2
Space group	$P4_32_12$
Wavelength (Å)	1.038
Unit-cell parameters (Å)	$a = b = 39.75$, $c = 141.83$
Total No. of reflections	821998
Unique reflections	47034
Completeness (%)	99.2 (97.5)
Resolution (Å)	99.0–1.10 (1.16–1.10)
$R_{\rm merge}$†	0.087 (0.676)
Multiplicity	17.5 (13.5)
Mosaicity (°)	0.22
Wilson B factor (Å^2)	8.7
$\langle I/\sigma(I)\rangle$	18.7 (4.0)

† $R_{\rm merge} = \sum_{hkl}\sum_i |I_i(hkl) - \langle I(hkl)\rangle| / \sum_{hkl}\sum_i I_i(hkl)$, where $I_i(hkl)$ is the intensity of an individual measurement of reflection i and $\langle I(hkl)\rangle$ is the mean intensity of the reflection.

Because the C-terminus of HINT1 (which mediates homodimer formation and nucleotide binding and exerts hydrolytic activity) is not responsible for interactions with other proteins, especially with transcription factors, it has been suggested that the N-terminus of HINT1 or some structural motifs from the N-terminal part only might be responsible for the formation of contacts with its binding partners (Cen *et al.*, 2009).

In this manuscript, we report the first detailed 1.10 Å structure of rabbit HINT1 in complex with adenosine.

2. Materials and methods

2.1. Cloning, expression and purification

Wild-type rHINT1 was expressed and purified in *E. coli* BL21 strain using the pSGA02-*HINT1* plasmid as described previously (Bieganowski *et al.*, 2002). Purification was performed using AMP–agarose (Sigma) affinity chromatography. A homogenous protein preparation was dialyzed against a buffer consisting of 20 m*M* Tris pH 7.5 and 150 m*M* NaCl, concentrated to a protein concentration of 10 mg ml^{-1}, frozen in liquid nitrogen and stored at 193 K.

2.2. Crystallization and data collection

rHINT1 was crystallized using the hanging-drop variant of the vapour-diffusion method at 278 K using 10 mg ml^{-1} protein solution and a precipitant solution consisting of 100 µ*M* sodium cacodylate buffer pH 6.5, 20–30%(*w*/*v*) PEG 8000 with or without the addition of 100 µ*M* sodium acetate. Crystallization drops were set up by mixing 2 µl protein solution with 2 µl precipitant solution and were suspended over 1 ml precipitant solution. Crystals of typical dimensions 0.1 × 0.2 × 0.6 mm with the shape of elongated tetragonal bipyramids appeared after 48–72 h.

Table 2
Final model-refinement statistics.

Resolution limits (Å)	38.27–1.10
No. of reflections used in refinement	44545
No. of reflections used for R_{free}	2371
R_{cryst}/R_{free}† (%)	14.25/16.77
No. of non-H atoms	
Protein	1024
Solvent	163
Ligand	19
R.m.s.d.s from ideal values	
Bond lengths (Å)	0.027
Bond angles (°)	2.489
Ramachandran plot‡	
Most favoured (%)	90.4
Additional allowed (%)	9.6
Mean B values§ (Å^2)	
Protein	14.87
Adenosine	19.54
Water	34.48

† $R_{cryst} = \sum_{hkl} \big||F_{obs}| - |F_{calc}|\big| / \sum_{hkl} |F_{obs}|$ for all reflections, where F_{obs} and F_{calc} are observed and calculated structure factors, respectively. R_{free} was calculated analogously for the test reflections, which were randomly selected and excluded from refinement. ‡ Calculated using *PROCHECK*. § Calculated using *BAVERAGE*.

Crystals of rHINT1 were flash-cooled by transfer into 25%(*v*/*v*) PEG 400 as a cryoprotectant followed by freezing in an N_2 stream at 100 K according to the procedure of Teng (1990). Diffraction data were collected using synchrotron radiation with a MAR CCD 165 mm detector on beamline I911-2 at the MAX-lab synchrotron, Lund, Sweden. The data were processed, integrated and scaled with *MOSFLM* and *SCALA* from the *CCP*4 package (Leslie, 1992; Winn *et al.*, 2011). Data-collection and processing statistics are given in Table 1. Assuming the presence of one molecule in the asymmetric unit, the Matthews coefficient V_M was 1.98 Å^3 Da^{-1}, corresponding to a solvent content of approximately 38%.

2.3. Structure determination and refinement

The diffraction data indicated the same space group as and practically identical unit-cell parameters to the previously published 1.80 Å resolution data (PDB entry 1rzy; Krakowiak *et al.*, 2004). The 1rzy structure was used directly as a search model in rigid-body refinement using the *REFMAC*5 program (Murshudov *et al.*, 2011). After the calculation of an initial electron-density map, the structure was completed using alternate cycles of manual building, including main-chain and side-chain rebuilding and the addition of alternative residue conformations, loop fragments and solvent molecules in the *Coot* program (Emsley *et al.*, 2010). Refinement was carried out with *REFMAC*5. All refinement steps were monitored using the R_{cryst} and R_{free} values. After the first few rounds of refinement, non-H atoms were refined anisotropically in all subsequent refinement cycles. During the first round of anisotropic refinement the R_{cryst} and R_{free} values fell considerably (approximately 4.5%) in comparison with isotropic refinement. The stereochemical quality of the resulting model was judged using the *PROCHECK* program (Laskowski *et al.*, 1993) and with validation tools implemented in *Coot*. Values of the mean temperature factors for protein main chain and side chains and water molecules were calculated using the *BAVERAGE* program from the *CCP*4 program suite (Winn *et al.*, 2011). Protein-structure superpositions were performed using the program *LSQKAB* (Kabsch, 1976). Graphic representations of superimposed structures were visually inspected. Interface analysis was performed using the EBI *PISA* server (Krissinel & Henrick, 2007; http://www.ebi.ac.uk/msd-srv/prot_int/pistart.html). Contacts were measured using the *CONTACT* program from *CCP*4. The refinement statistics of the described structure are given in Table 2.

3. Results and discussion

3.1. Quality of the model

rHINT1 crystallized in a tetragonal space group with one crystallographically independent molecule in the asymmetric unit. The structure of rHINT1 was refined to 1.10 Å resolution with anisotropic B factors for all non-H atoms. The refinement process converged to an R_{cryst} of 14.25% for all 44 545 reflections. The last recorded R_{free} was 16.77% for 2371 reflections. The refined model contained 1024 protein atoms from a single protein chain, 163 fully occupied water molecules and one molecule of adenosine per asymmetric unit. The first 12 residues at the N-terminus could not be modelled in the structure owing to a lack of sufficient density, similar to other available HINT1 structures. All of the remaining residues are characterized by very well defined electron density in the $2F_o - F_c$ map. For several residues, especially serines and methionines, alternative conformations have been observed. The r.m.s. deviations (r.m.s.d.s) in bond lengths and bond angles were 0.027 Å and 2.489°, respectively. These values are above the generally accepted limits, but similar r.m.s. deviations have been obtained for parallel refined structures of rHINT1 cysteine mutants (PDB codes 3o1c, 3o1x and 3o1z; Ozga *et al.*, 2010). This observation indicates overweighting of the X-ray data and may suggest some problems with the automatic weighting option used during structure refinement; however, recently published opinions have suggested that higher r.m.s.d. values should be accepted for high-resolution structures (Jaskolski *et al.*, 2007). The average B factors for protein atoms, adenosine and water molecules were 14.87, 19.54 and 34.48 Å^2, respectively.

The Ramachandran plot (φ, ψ) showed that 90.4% of non-Gly and non-Pro residues were in most favoured regions and 9.6% fell into additionally allowed regions. No residues were in generously allowed or disallowed regions. 13 amino-acid residues (Phe19, Asp36, Ser45, Ile63, Glu67, Ser72, Met78, Tyr94, Met96, Ser102, Ser107, Val111 and Asn122) were modelled in alternative conformations. A fragment of the L1 loop (amino acids 27–30) was modelled in alternative positions according to peaks in an $F_o - F_c$ positive electron-density map contoured at the 3σ level. Analysis with the *ERRAT* program (Colovos & Yeates, 1993) gives an overall quality factor of 98.1%, which is good for a 1.10 Å resolution structure.

3.2. Nucleotide-binding site

Previously published ligand-binding studies have shown that HINT proteins are able to bind purine nucleosides and nucleotides despite the fact that the HINT nucleotide-binding motif possesses a different sequence in comparison with other nucleotide-binding proteins (Gilmour *et al.*, 1997). In the PDB, the following HINT1–ligand complex structures are available: with AMP (PDB entry 1kpf; Lima *et al.*, 1997), GMP (PDB entry 3rhn; Brenner *et al.*, 1997), 8-Br-AMP (PDB entry 5rhn; Brenner *et al.*, 1997), adenosine 5′-*O*-(α/β-methylenediphosphonate) (PDB entry 1av5; Lima *et al.*, 1997), adenosine 5′-ditungstate (PDB entry 1kpe; Lima *et al.*, 1997) and 5′-*O*-(*N*-ethylsulfamoyl)adenosine (PDB entry 1rzy; Krakowiak *et al.*, 2004). The structure reported here (PDB enry 3qgz) is the first published high-resolution structure of a complex of rHINT1 with adenosine. The only previously deposited structure of an rHINT1–adenosine complex (PDB code 4rhn; Brenner *et al.*, 1997) has an incomplete ligand (only the ribose residue is visible) in the binding pocket, probably because of the limited data resolution.

The location of adenosine, which was used during elution of the protein from the affinity column in the purification step and remained inside the binding pocket after dialysis, was clearly identified in the $F_o - F_c$ electron-density map and the ligand model was easily fitted, but a small discontinuity in the region of the adenine ring was indicated in the map, probably because of possible partial occupancy as well as mobility of the molecule. However, the $2F_o - F_c$ map calculated after refinement covers the fully occupied ligand completely, confirming its correct placement and occupancy (Fig. 3). The base-binding region is formed by the most hydrophobic environment, which is composed of four isoleucine residues (Ile18, Ile22, Ile27 and Ile44) and two phenylalanine residues (Phe19 and Phe41). Additionally, the base position is stabilized by hydrogen bonds through structural water molecules that are present in the cleft and interact with the Pro28 and Glu34 carbonyl O atoms. The ribose residue is bound by hydrogen-bond interactions with the Asp43 residue and, *via* a water molecule, with the Ser45 carbonyl O atom. The O5′ atom of the ribose makes a strong hydrogen-bond contact with the His112 residue and additionally with three water molecules, which form a hydrogen-bond network with amino-acid residues of the HINT protein active centre (Fig. 4).

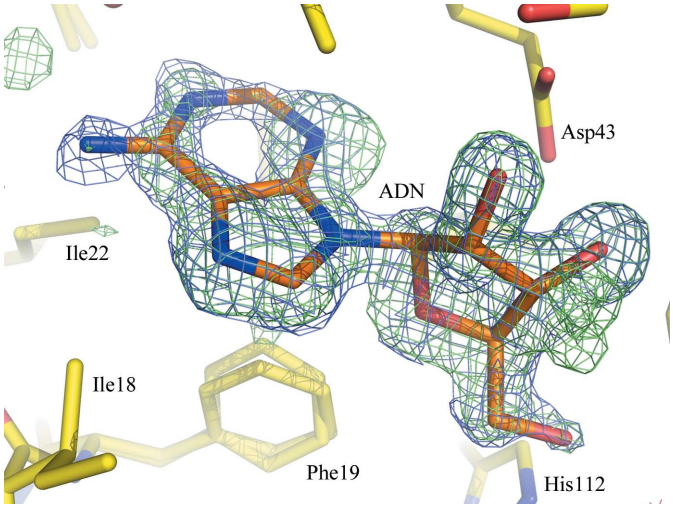

Figure 3
$2F_o - F_c$ electron-density map contoured at the 1.0σ level and OMIT $F_o - F_c$ electron-density map contoured at the 3.0σ level of the adenosine molecule (ADN) from 1.10 Å resolution data (PDB entry 3qgz). This figure was created with *PyMOL* v.0.99 (DeLano Scientific, Palo Alto, California, USA).

3.3. Structural comparison

The overall shape of the obtained rHINT1 structure model is almost identical to the 1rzy model and its fold is almost identical to other HINT1 structures deposited in the PDB. Least-squares superposition of the C^{α} coordinates of the rHINT1 monomer at 1.10 Å resolution with those published previously (PDB code 1rzy; Krakowiak *et al.*, 2004) at 1.80 Å resolution reveals a close resemblance between the compared structures, with an r.m.s.d. of 0.09 Å. The high-resolution data allow updating of the previously deposited model and the building of a more detailed rHINT1 structure model with higher precision. Some residues which were not recognized previously were now visible and were easy to interpret and fit into electron-density maps (Asp16 and Lys91). For many

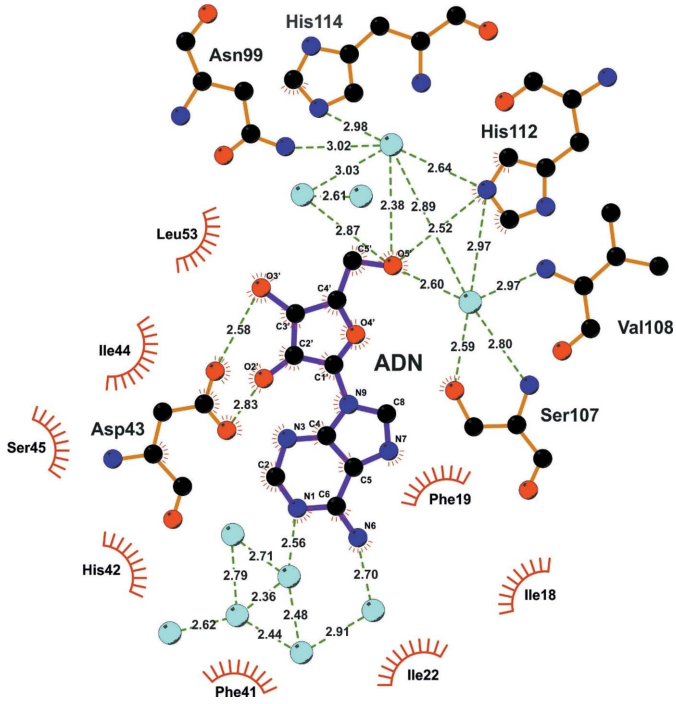

Figure 4
Schematic diagram of the binding site of the rHINT1–adenosine complex. Hydrogen-bonding interactions between adenosine atoms and nearby side chains or water molecules are shown as dashed lines and the distances are shown in Å. Residues making hydrophobic contacts to the ligand are indicated as shown at the bottom and right. C atoms are shown in black, O atoms in red and N atoms in blue. Water molecules are shown in cyan. Covalent bonds within the ligand are drawn with purple lines, while those within the protein are drawn with orange lines. The adenosine is labelled 'ADN'. This diagram was prepared with *LIGPLOT* (Wallace *et al.*, 1996).

amino-acid residues two or more alternative rotamer positions were observed: Phe19, Lys25, Asp36, Leu39, Ile63, Glu67, Ser72, Met78, Tyr94, Met96, Ser102 and Ser107. The protein model was completed by the addition of almost 100 water molecules.

One interesting fact was the observation of the L1 loop fragment (amino acids 27–30). This part of the protein chain, which is involved in building the binding cleft, has potential to change its conformation. The largest shift, of about 2.20 Å, was measured for the Pro28 residue and this displacement is visible in the structure presented here as a fragment modelled in two conformations (Fig. 5). In addition, superposition of the present rHINT1 structure on other HINT1 structures deposited in the PDB shows that the L1 loop region also shows flexibility between the compared models (Fig. 6). However, analysis of superposed HINT1 structures did not show significant differences in the placement of ligands inside the binding pocket. Additionally, the geometries of superposed models of rabbit and human HINT1 are practically identical, in contrast to *E. coli* HINT1, in which a different structure of the main chain is visible in the N- and C-terminal regions.

Analysis of the average temperature (*B*) factors calculated for the main and side chains and their visualization (Fig. 7) confirms the observation of disordered or highly flexible regions, including the fragment of loop L1 described above and the N-terminal fragment. This effect could be responsible for the problems in the determination of the positions of the first 12 amino-acid residues, which are invisible in the obtained high-resolution electron-density maps, possibly because of the high flexibility of this N-terminal fragment. The remaining parts of the protein structure did not exhibit significant differences in *B*-factor values; this is visible in the quality of the obtained electron-density maps, which did not cause difficulties in interpretation during fitting and rebuilding of the model.

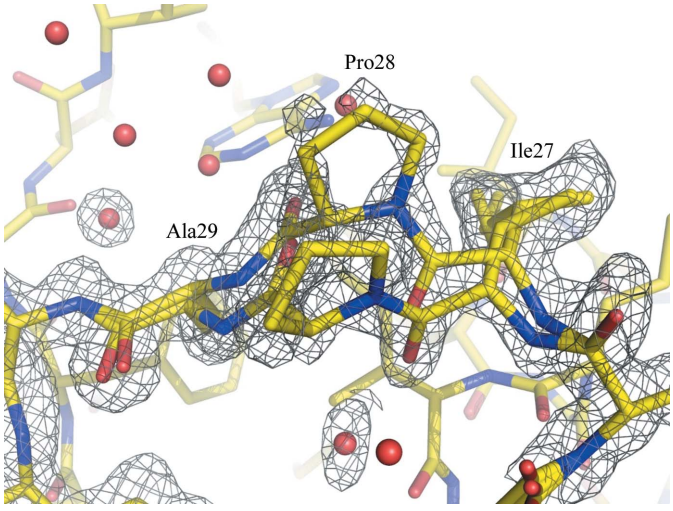

Figure 5
Displacement of the L1 loop (amino acids 27–30). The protein model is shown in stick representation with a $2F_o - F_c$ electron-density map contoured at the 1.0σ level calculated from 1.10 Å resolution data (PDB entry 3qgz). This figure was created with *PyMOL* v.0.99 (DeLano Scientific, Palo Alto, California, USA).

4. Conclusions

The crystal structure of rHINT1 in complex with adenosine was determined at 1.10 Å resolution and is currently the highest resolution wild-type HINT1 structure to be obtained. Anisotropic refinement of the non-H atoms resulted in a final structure with good crystallographic statistics and stereochemical quality. The presented structure is the first complete

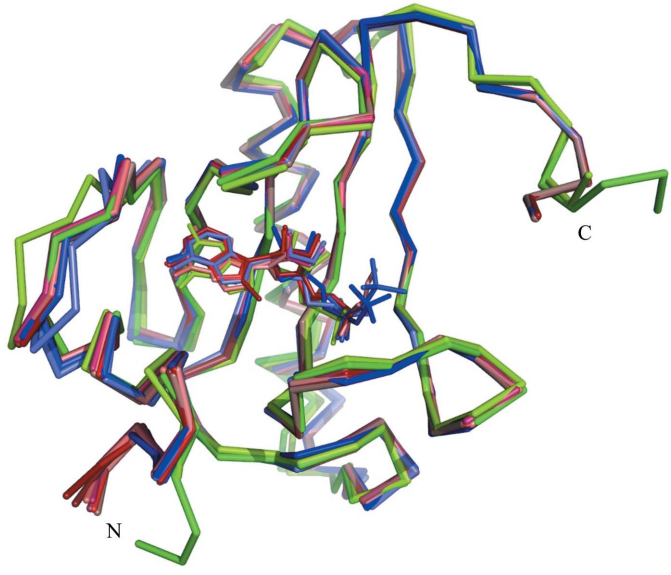

Figure 6
Superposition of the C^{α} atoms of rabbit (red), human (blue) and bacterial (green) HINT1 structures deposited in the PDB. Calculations were made in *LSQKAB* (Kabsch, 1976). This figure was created with *PyMOL* v.0.99 (DeLano Scientific, Palo Alto, California, USA).

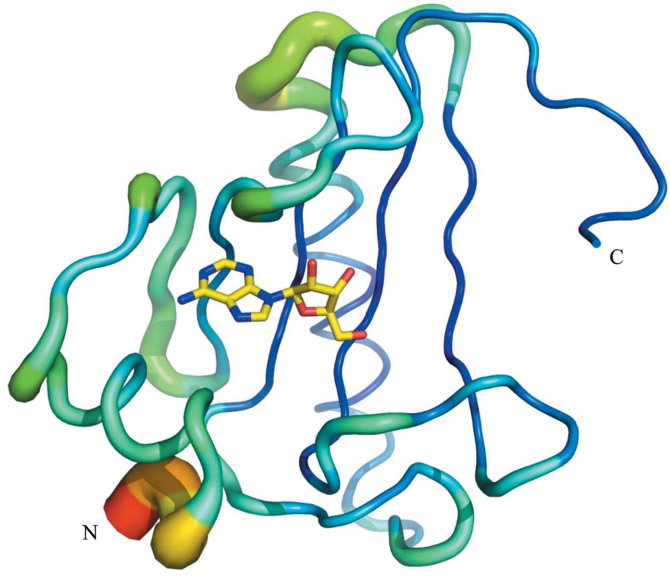

Figure 7
'Sausage' representation of the main-chain *B*-factor distribution of the described rHINT1 structure. *B*-factor values are indicated from the lowest (blue) to the highest level (red). This figure was created with *PyMOL* v.0.99 (DeLano Scientific, Palo Alto, California, USA).

description of a complex of HINT1 with a purine nucleoside, in contrast to other existing HINT1 structures complexed with nucleotides or nucleotide analogues. The structure shows that the binding of adenosine in the binding cleft does not lead to significant conformational changes in comparison with the structures of other HINT1 complexes, except for the fragment of the L1 loop involved in the formation of the nucleotide-binding cavity. Unfortunately, even these excellent resolution data do not allow definition of the structure of the N-terminal fragment of rHINT1.

This project was financially assisted by the Polish Ministry of Science and Higher Education grants NN204516139 (to RD) for the years 2010–2013 and PBZ-MNiSW-07/I/2007 (to BN) for the years 2008–2010. We would like to thanks Grzegorz Bujacz and members of his team (Technical University of Lodz, Faculty of Food Chemistry and Biotechnology, Institute of Technical Biochemistry) for support with synchrotron data collection at MAX-Lab, Lund, Sweden.

References

Ahel, I., Rass, U., El-Khamisy, S. F., Katyal, S., Clements, P. M., McKinnon, P. J., Caldecott, K. W. & West, S. C. (2006). *Nature (London)*, **443**, 713–716.

Bardaweel, S., Pace, J., Chou, T.-F., Cody, V. & Wagner, C. R. (2010). *J. Mol. Biol.* **404**, 627–638.

Barnes, L. D., Garrison, P. N., Siprashvili, Z., Guranowski, A., Robinson, A. K., Ingram, S. W., Croce, C. M., Ohta, M. & Huebner, K. (1996). *Biochemistry*, **35**, 11529–11535.

Bieganowski, P., Garrison, P. N., Hodawadekar, S. C., Faye, G., Barnes, L. D. & Brenner, C. (2002). *J. Biol. Chem.* **277**, 10852–10860.

Boulanger, R. R. & Kantrowitz, E. R. (2003). *J. Biol. Chem.* **278**, 23497–23501.

Brenner, C. (2002). *Biochemistry*, **41**, 9003–9014.

Brenner, C., Garrison, P., Gilmour, J., Peisach, D., Ringe, D., Petsko, G. A. & Lowenstein, J. M. (1997). *Nature Struct. Biol.* **4**, 231–238.

Cen, B., Li, H. & Weinstein, I. B. (2009). *J. Biol. Chem.* **284**, 5265–5276.

Chou, T.-F., Bieganowski, P., Shilinski, K., Cheng, J., Brenner, C. & Wagner, C. R. (2005). *J. Biol. Chem.* **280**, 15356–15361.

Chou, T.-F., Tikh, I. B., Horta, B. A., Ghosh, B., De Alencastro, R. B. & Wagner, C. R. (2007). *J. Biol. Chem.* **282**, 15137–15147.

Chou, T.-F. & Wagner, C. R. (2007). *J. Biol. Chem.* **282**, 4719–4727.

Colovos, C. & Yeates, T. O. (1993). *Protein Sci.* **2**, 1511–1519.

Date, H. *et al.* (2001). *Nature Genet.* **29**, 184–188.

Emsley, P., Lohkamp, B., Scott, W. G. & Cowtan, K. (2010). *Acta Cryst.* D**66**, 486–501.

Gilmour, J., Liang, N. & Lowenstein, J. M. (1997). *Biochem. J.* **326**, 471–477.

Guang, W., Wang, H., Su, T., Weinstein, I. B. & Wang, J. B. (2004). *Mol. Pharmacol.* **66**, 1285–1292.

Guranowski, A., Wojdyła, A. M., Rydzik, A. M., Stepiński, J. & Jemielity, J. (2011). *Acta Biochim. Pol.* **58**, 131–136.

Hsieh, S.-Y., Hsu, C.-Y., He, J.-R., Liu, C.-L., Lo, S.-J., Chen, Y.-C. & Huang, H.-Y. (2009). *J. Proteome Res.* **8**, 3977–3986.

Huang, K., Arabshahi, A. & Frey, P. A. (2005). *Eur. J. Org. Chem.* **2005**, 5198–5206.

Jaskolski, M., Gilski, M., Dauter, Z. & Wlodawer, A. (2007). *Acta Cryst.* D**63**, 611–620.

Kabsch, W. (1976). *Acta Cryst.* A**32**, 922–923.

Kabsch, W. & Sander, C. (1983). *Biopolymers*, **22**, 2577–2637.

Kijas, A. W., Harris, J. L., Harris, J. M. & Lavin, M. F. (2006). *J. Biol. Chem.* **281**, 13939–13948.

Klein, M. G., Yao, Y., Slosberg, E. D., Lima, C. D., Doki, Y. & Weinstein, I. B. (1998). *Exp. Cell Res.* **244**, 26–32.

Korsisaari, N., Rossi, D. J., Luukko, K., Huebner, K., Henkemeyer, M. & Mäkelä, T. P. (2003). *Mol. Cell. Biol.* **23**, 3929–3935.

Krakowiak, A., Kaczmarek, R., Baraniak, J., Wieczorek, M. & Stec, W. J. (2007). *Chem. Commun.*, pp. 2163–2165.

Krakowiak, A., Pace, H. C., Blackburn, G. M., Adams, M., Mekhalfia, A., Kaczmarek, R., Baraniak, J., Stec, W. J. & Brenner, C. (2004). *J. Biol. Chem.* **279**, 18711–18716.

Krissinel, E. & Henrick, K. (2007). *J. Mol. Biol.* **372**, 774–797.

Laskowski, R. A., MacArthur, M. W., Moss, D. S. & Thornton, J. M. (1993). *J. Appl. Cryst.* **26**, 283–291.

Lee, Y.-N., Nechushtan, H., Figov, N. & Razin, E. (2004). *Immunity*, **20**, 145–151.

Lee, Y.-N. & Razin, E. (2005). *Mol. Cell. Biol.* **25**, 8904–8912.

Leslie, A. G. W. (1992). *Jnt CCP4/ESF–EACBM Newsl. Protein Crystallogr.* **26**.

Li, H., Zhang, Y., Su, T., Santella, R. M. & Weinstein, I. B. (2006). *Oncogene*, **25**, 713–721.

Lima, C. D., Klein, M. G. & Hendrickson, W. A. (1997). *Science*, **278**, 286–290.

Lima, C. D., Klein, M. G., Weinstein, I. B. & Hendrickson, W. A. (1996). *Proc. Natl Acad. Sci. USA*, **93**, 5357–5362.

Liu, H., Rodgers, N. D., Jiao, X. & Kiledjian, M. (2002). *EMBO J.* **21**, 4699–4708.

Moreira, M. C. *et al.* (2001). *Nature Genet.* **29**, 189–193.

Murakami, E., Tolstykh, T., Bao, H., Niu, C., Micolochick Steuer, H. M., Bao, D., Chang, W., Espiritu, C., Bansal, S., Lam, A. M., Otto, M. J., Sofia, M. J. & Furman, P. A. (2010). *J. Biol. Chem.* **285**, 34337–34347.

Murshudov, G. N., Skubák, P., Lebedev, A. A., Pannu, N. S., Steiner, R. A., Nicholls, R. A., Winn, M. D., Long, F. & Vagin, A. A. (2011). *Acta Cryst.* D**67**, 355–367.

Ohta, M., Inoue, H., Cotticelli, M. G., Kastury, K., Baffa, R., Palazzo, J., Siprashvili, Z., Mori, M., McCue, P., Druck, T., Croce, C. M. & Huebner, K. (1996). *Cell*, **84**, 587–597.

Ozga, M., Dolot, R., Janicka, M., Kaczmarek, R. & Krakowiak, A. (2010). *J. Biol. Chem.* **285**, 40809–40818.

Parks, K. P., Seidle, H., Wright, N., Sperry, J. B., Bieganowski, P., Howitz, K., Wright, D. L. & Brenner, C. (2004). *Physiol. Genomics*, **20**, 12–14.

Pearson, J. D., DeWald, D. B., Mathews, W. R., Mozier, N. M., Zürcher-Neely, H. A., Heinrikson, R. L., Morris, M. A., McCubbin, W. D., McDonald, J. R. & Fraser, E. D. (1990). *J. Biol. Chem.* **265**, 4583–4591.

Su, T., Suzui, M., Wang, L., Lin, C.-S., Xing, W.-Q. & Weinstein, I. B. (2003). *Proc. Natl Acad. Sci. USA*, **100**, 7824–7829.

Teng, T.-Y. (1990). *J. Appl. Cryst.* **23**, 387–391.

Wallace, A. C., Laskowski, R. A. & Thornton, J. M. (1996). *Protein Eng.* **8**, 127–134.

Wang, L., Li, H., Zhang, Y., Santella, R. M. & Weinstein, I. B. (2009). *Int. J. Cancer*, **124**, 1526–1534.

Wang, L., Zhang, Y., Li, H., Xu, Z., Santella, R. M. & Weinstein, I. B. (2007). *Cancer Res.* **67**, 4700–4708.

Weiske, J. & Huber, O. (2005). *J. Cell Sci.* **118**, 3117–3129.

Weiske, J. & Huber, O. (2006). *J. Biol. Chem.* **281**, 27356–27366.

Winn, M. D. *et al.* (2011). *Acta Cryst.* D**67**, 235–242.

Wu, L., Wu, X., Deng, H. & Huang, Y. (2010). *Dev. Comp. Immunol.* **34**, 76–83.

Zambelli, D., Zuntini, M., Nardi, F., Manara, M. C., Serra, M., Landuzzi, L., Lollini, P. L., Ferrari, S., Alberghini, M., Llombart-Bosch, A., Piccolo, E., Iacobelli, S., Picci, P. & Scotlandi, K. (2010). *Int. J. Cancer*, **126**, 41–52.

Zhang, Y.-J., Li, H., Wu, H.-C., Shen, J., Wang, L., Yu, M.-W., Lee, P.-H., Weinstein, I. B. & Santella, R. M. (2009). *Cancer Lett.* **275**, 277–284.